Research Article | Vol. 8, No. 7 | 1 Jul 2017 | BIOMEDICAL OPTICS EXPRESS 3426
Biomedical Optics EXPRESS

In vivo analysis of mucosal lipids reveals histological disease activity in ulcerative colitis using endoscope-coupled Raman spectroscopy

HAO DING,[1] ANDREW W. DUPONT,[2] SHASHIDEEP SINGHAL,[2] LARRY D. SCOTT,[2] SUSHOVAN GUHA,[2] MAMOUN YOUNES,[3] AND XIAOHONG BI[1,*]

[1]*Center for Precision Biomedicine, Institute of Molecular Medicine, McGovern Medical School, the University of Texas Health Science Center at Houston, 1881 East Road, Houston, TX 77054, USA*
[2]*Division of Gastroenterology, Hepatology and Nutrition, Department of Internal Medicine, McGovern Medical School, the University of Texas Health Science Center at Houston, 6431 Fannin Street, Houston, Texas 77030, USA*
[3]*Department of Pathology & Laboratory Medicine, McGovern Medical School, the University of Texas Health Science Center at Houston, 6431 Fannin Street, Houston, Texas 77030, USA*
[*]*Xiaohong.bi@uth.tmc.edu*

Abstract: The goal of this study is to evaluate endoscopic Raman spectroscopy as a noninvasive technique to determine histological inflammatory status of colitis. Colon mucosal composition was investigated *in vivo* from patients with ulcerative colitis (UC) and from age- and body mass index (BMI) matched controls using endoscope-coupled Raman spectroscopy. The results were co-registered with histological assessment of inflammatory status at the same locations. Substantial decreases (50-60%) in the content of phosphotidylcholines (PCs) and total lipids were observed in inflamed colon tissue (histology grade 1, 2 and 3) compared to those from the quiescent (histology grade 0) and from the controls. No significant difference was observed in lipids or PC contents between control and grade 0, or among grades 1 – 3. The degree of lipid unsaturation increased in the inflamed tissue regardless of disease severity. The inflammation-associated alterations in lipids and PC are observed independent of BMI or the anatomical locations for data collection. Multivariate analysis using support vector machine (SVM) algorithm classified the spectra of the controls or the inactive colitis from those of inflamed tissue with a sensitivity of 83.5% and 97.1% respectively. Our results showed that mucosal lipid content is related to the microscopic disease activity, and thus could serve as a valuable spectral marker to differentiate active colitis from the quiescent.

OCIS codes: (170.5660) Raman spectroscopy; (170.2150) Endoscopic imaging; (170.2680) Gastrointestinal.

References and links

1. E. V. Loftus, Jr., "Clinical epidemiology of inflammatory bowel disease: Incidence, prevalence, and environmental influences," Gastroenterology **126**(6), 1504–1517 (2004).
2. J. Misiewicz, J. Lennard-Jones, A. Connell, J. Baron, and F. A. Jones, "Controlled trial of sulphasalazine in maintenance therapy for ulcerative colitis," Lancet **285**(7378), 185–188 (1965).
3. M. A. Kamm, "Review article: maintenance of remission in ulcerative colitis," Aliment. Pharmacol. Ther. **16**(Suppl 4), 21–24 (2002).
4. G. D'Haens, W. J. Sandborn, B. G. Feagan, K. Geboes, S. B. Hanauer, E. J. Irvine, M. Lémann, P. Marteau, P. Rutgeerts, J. Schölmerich, and L. R. Sutherland, "A review of activity indices and efficacy end points for clinical trials of medical therapy in adults with ulcerative colitis," Gastroenterology **132**(2), 763–786 (2007).
5. A. Orlando, F. W. Guglielmi, M. Cottone, E. Orlando, C. Romano, and E. Sinagra, "Clinical implications of mucosal healing in the management of patients with inflammatory bowel disease," Dig. Liver Dis. **45**(12), 986–991 (2013).
6. M. Cintolo, G. Costantino, S. Pallio, and W. Fries, "Mucosal healing in inflammatory bowel disease: Maintain or de-escalate therapy," World J. Gastrointest. Pathophysiol. **7**(1), 1–16 (2016).

#294862 https://doi.org/10.1364/BOE.8.003426
Journal © 2017 Received 4 May 2017; revised 5 Jun 2017; accepted 7 Jun 2017; published 23 Jun 2017

Biomedical Optics EXPRESS

7. A. Tursi, W. Elisei, M. Picchio, G. Forti, A. Penna, C. D. Inchingolo, R. Nenna, and G. Brandimarte, "Histological inflammation in ulcerative colitis in deep remission under treatment with infliximab," Clin. Res. Hepatol. Gastroenterol. **39**(1), 107–113 (2015).
8. M. Rutter, B. Saunders, K. Wilkinson, S. Rumbles, G. Schofield, M. Kamm, C. Williams, A. Price, I. Talbot, and A. Forbes, "Severity of inflammation is a risk factor for colorectal neoplasia in ulcerative colitis," Gastroenterology **126**(2), 451–459 (2004).
9. R. B. Gupta, N. Harpaz, S. Itzkowitz, S. Hossain, S. Matula, A. Kornbluth, C. Bodian, and T. Ullman, "Histologic inflammation is a risk factor for progression to colorectal neoplasia in ulcerative colitis: a cohort study," Gastroenterology **133**(4), 1099–1105 (2007).
10. X. Bi, A. Walsh, A. Mahadevan-Jansen, and A. Herline, "Development of spectral markers for the discrimination of ulcerative colitis and Crohn's disease using Raman spectroscopy," Dis. Colon Rectum **54**(1), 48–53 (2011).
11. M. Marro, A. Taubes, A. Abernathy, S. Balint, B. Moreno, B. Sanchez-Dalmau, E. H. Martínez-Lapiscina, I. Amat-Roldan, D. Petrov, and P. Villoslada, "Dynamic molecular monitoring of retina inflammation by in vivo Raman spectroscopy coupled with multivariate analysis," J. Biophotonics **7**(9), 724–734 (2014).
12. I. Pence, Q. Nguyen, X. Bi, A. Herline, D. Beaulieu, S. Horst, D. Schwartz, and A. Mahadevan-Jansen, "Endoscopy-coupled Raman spectroscopy for in vivo discrimination of inflammatory bowel disease." in *SPIE BiOS*. 2014. International Society for Optics and Photonics.
13. H. Ding, M. Cao, A.W. DuPont, L.D. Scott, S. Guha, S. Singhal, M. Younes, I. Pence, A. Herline, D. Schwartz, H. Xu, A. Mahadevan-Jansen, and X. Bi, "Discrimination of inflammatory bowel disease using Raman spectroscopy and linear discriminant analysis methods," Proc. SPIE **9704**, 97040W (2016).
14. I. J. Pence, D. B. Beaulieu, S. N. Horst, X. Bi, A. J. Herline, D. A. Schwartz, and A. Mahadevan-Jansen, "Clinical characterization of in vivo inflammatory bowel disease with Raman spectroscopy," Biomed. Opt. Express **8**(2), 524–535 (2017).
5. H. Ding, A. W. DuPont, S. Singhal, L. D. Scott, S. Guha, M. Younes, Y. Ye, and X. Bi, "Effect of physiological factors on the biochemical properties of colon tissue – an in vivo Raman spectroscopy study," J. Raman Spectrosc. (2017).
16. C.f, D.C.a. Prevention. "About Adult Body Mass Index (BMI)," Available from: https://www.cdc.gov/healthyweight/assessing/bmi/adult_bmi/index.html.
17. M. G. Shim, L. M. Song, N. E. Marcon, and B. C. Wilson, "In vivo near-infrared Raman spectroscopy: demonstration of feasibility during clinical gastrointestinal endoscopy," Photochem. Photobiol. **72**(1), 146–150 (2000).
18. I. J. Pence, E. Vargis, and A. Mahadevan-Jansen, "Assessing variability of in vivo tissue Raman spectra," Appl. Spectrosc. **67**(7), 789–800 (2013).
19. B. Lemmens, I. Arijs, G. Van Assche, X. Sagaert, K. Geboes, M. Ferrante, P. Rutgeerts, S. Vermeire, and G. De Hertogh, "Correlation between the endoscopic and histologic score in assessing the activity of ulcerative colitis," Inflamm. Bowel Dis. **19**(6), 1194–1201 (2013).
20. C. A. Lieber, S. K. Majumder, D. L. Ellis, D. D. Billheimer, and A. Mahadevan-Jansen, "In vivo nonmelanoma skin cancer diagnosis using Raman microspectroscopy," Lasers Surg. Med. **40**(7), 461–467 (2008).
21. R. Ellis, E. Green, and C. P. Winlove, "Structural analysis of glycosaminoglycans and proteoglycans by means of Raman microspectrometry," Connect. Tissue Res. **50**(1), 29–36 (2009).
22. B. Mortada, E.-S. M. El-Rabaie, M. F. El-Kordy, O. Zahran, and F. E. A. El-Samie, "Trend removal from Raman spectra with local variance estimation adn cubic spline interpolation," Circuits and Systems: An International Journal **2**(1), 12 (2015).
23. C. Krafft, L. Neudert, T. Simat, and R. Salzer, "Near infrared Raman spectra of human brain lipids," Spectrochim. Acta A Mol. Biomol. Spectrosc. **61**(7), 1529–1535 (2005).
24. I. Notingher, C. Green, C. Dyer, E. Perkins, N. Hopkins, C. Lindsay, and L. L. Hench, "Discrimination between ricin and sulphur mustard toxicity in vitro using Raman spectroscopy," J. R. Soc. Interface **1**(1), 79–90 (2004).
25. K. G. Brown, W. L. Peticolos, and E. Brown, "Raman studies of conformational changes in model membrane systems," Biochem. Biophys. Res. Commun. **54**(1), 358–364 (1973).
26. G. J. Thomas, Jr., J. M. Benevides, S. A. Overman, T. Ueda, K. Ushizawa, M. Saitoh, and M. Tsuboi, "Polarized Raman spectra of oriented fibers of A DNA and B DNA: anisotropic and isotropic local Raman tensors of base and backbone vibrations," Biophys. J. **68**(3), 1073–1088 (1995).
27. K. Czamara, K. Majzner, M. Z. Pacia, K. Kochan, A. Kaczor, and M. Baranska, "Raman spectroscopy of lipids: a review," J. Raman Spectrosc. **46**(1), 4–20 (2015).
28. B. P. Gaber, W. L. Peticolas, "On the quantitative interpretation of biomembrane structure by Raman spectroscopy," Biochimica et Biophysica Acta (BBA) - Biomembranes **465**(2), 260–274 (1977).
29. P. Chen, F. Zhang, G. Mu, G. Tang, H. Zhao, H. Bai, H. Fang, L. Lin, L. Zhang, and W. Gong, "Raman spectroscopy for noninvasive monitoring of umbilical cord mesenchymal stem cells viability transitions," in *Stem Cells in Clinic and Research*, A. Gholamrezanezhad, ed. (INTECH Open Access Publisher, 2011).
30. K. Czamara, K. Majzner, A. Selmi, M. Baranska, Y. Ozaki, and A. Kaczor, "Unsaturated lipid bodies as a hallmark of inflammation studied by Raman 2D and 3D microscopy," Sci. Rep. **7**, 40889 (2017).
31. M. S. Bergholt, W. Zheng, K. Lin, J. Wang, H. Xu, J. L. Ren, K. Y. Ho, M. Teh, K. G. Yeoh, and Z. Huang, "Characterizing variability of in vivo Raman spectroscopic properties of different anatomical sites of normal colorectal tissue towards cancer diagnosis at colonoscopy," Anal. Chem. **87**(2), 960–966 (2015).

Biomedical Optics EXPRESS

32. M. S. Bergholt, K. Lin, J. Wang, W. Zheng, H. Xu, Q. Huang, J. L. Ren, K. Y. Ho, M. Teh, S. Srivastava, B. Wong, K. G. Yeoh, and Z. Huang, "Simultaneous fingerprint and high-wavenumber fiber-optic Raman spectroscopy enhances real-time in vivo diagnosis of adenomatous polyps during colonoscopy," J. Biophotonics **9**(4), 333–342 (2016).
33. M. A. Short, W. Wang, I. T. Tai, and H. Zeng, "Development and in vivo testing of a high frequency endoscopic Raman spectroscopy system for potential applications in the detection of early colonic neoplasia," J. Biophotonics **9**(1-2), 44–48 (2015).
34. M. A. Short, I. T. Tai, D. Owen, and H. Zeng, "Using high frequency Raman spectra for colonic neoplasia detection," Opt. Express **21**(4), 5025–5034 (2013).
35. C. Atuma, V. Strugala, A. Allen, and L. Holm, "The adherent gastrointestinal mucus gel layer: thickness and physical state in vivo," Am. J. Physiol. Gastrointest. Liver Physiol. **280**(5), G922–G929 (2001).
36. M. E. Johansson, J. M. Larsson, and G. C. Hansson, "The two mucus layers of colon are organized by the MUC2 mucin, whereas the outer layer is a legislator of host-microbial interactions," Proc. Natl. Acad. Sci. U.S.A. **108**(Suppl 1), 4659–4665 (2011).
37. L. M. Lichtenberger, "The hydrophobic barrier properties of gastrointestinal mucus," Annu. Rev. Physiol. **57**(1), 565–583 (1995).
38. R. Ehehalt, A. Braun, M. Karner, J. Füllekrug, and W. Stremmel, "Phosphatidylcholine as a constituent in the colonic mucosal barrier--physiological and clinical relevance," Biochim. Biophys. Acta **1801**(9), 983–993 (2010).
39. R. T. Spychal, J. M. Marrero, S. H. Saverymuttu, and T. C. Northfield, "Measurement of the surface hydrophobicity of human gastrointestinal mucosa," Gastroenterology **97**(1), 104–111 (1989).
40. A. Braun, U. Schönfeld, T. Welsch, M. Kadmon, B. Funke, D. Gotthardt, A. Zahn, F. Autschbach, P. Kienle, M. Zharnikov, M. Grunze, W. Stremmel, and R. Ehehalt, "Reduced hydrophobicity of the colonic mucosal surface in ulcerative colitis as a hint at a physicochemical barrier defect," Int. J. Colorectal Dis. **26**(8), 989–998 (2011).
41. R. Ehehalt, J. Wagenblast, G. Erben, W. D. Lehmann, U. Hinz, U. Merle, and W. Stremmel, "Phosphatidylcholine and lysophosphatidylcholine in intestinal mucus of ulcerative colitis patients. A quantitative approach by nanoElectrospray-tandem mass spectrometry," Scand. J. Gastroenterol. **39**(8), 737–742 (2004).
42. A. Braun, I. Treede, D. Gotthardt, A. Tietje, A. Zahn, R. Ruhwald, U. Schoenfeld, T. Welsch, P. Kienle, G. Erben, W. D. Lehmann, J. Fuellekrug, W. Stremmel, and R. Ehehalt, "Alterations of phospholipid concentration and species composition of the intestinal mucus barrier in ulcerative colitis: a clue to pathogenesis," Inflamm. Bowel Dis. **15**(11), 1705–1720 (2009).
43. J. Addis, N. Mohammed, O. Rotimi, D. Magee, A. Jha, and V. Subramanian, "Raman spectroscopy of endoscopic colonic biopsies from patients with ulcerative colitis to identify mucosal inflammation and healing," Biomed. Opt. Express **7**(5), 2022–2035 (2016).
44. R. D. Pullan, G. A. Thomas, M. Rhodes, R. G. Newcombe, G. T. Williams, A. Allen, and J. Rhodes, "Thickness of adherent mucus gel on colonic mucosa in humans and its relevance to colitis," Gut **35**(3), 353–359 (1994).
45. G. F. Cope, R. V. Heatley, J. Kelleher, and A. T. Axon, "In vitro mucus glycoprotein production by colonic tissue from patients with ulcerative colitis," Gut **29**(2), 229–234 (1988).
46. S. D. Ryder, A. H. Raouf, N. Parker, R. J. Walker, and J. M. Rhodes, "Abnormal Mucosal Glycoprotein Synthesis in Inflammatory Bowel Diseases is not Related to Cigarette Smoking," Digestion **56**(5), 370–376 (1995).
47. R. P. MacDermott, R. M. Donaldson, Jr., and J. S. Trier, "Glycoprotein synthesis and secretion by mucosal biopsies of rabbit colon and human rectum," J. Clin. Invest. **54**(3), 545–554 (1974).
48. A. E. Dorofeyev, I. V. Vasilenko, O. A. Rassokhina, and R. B. Kondratiuk, "Mucosal barrier in ulcerative colitis and Crohn's disease," Gastroenterol. Res. Pract. **2013**, 431231 (2013).
49. V. Strugala, P. W. Dettmar, and J. P. Pearson, "Thickness and continuity of the adherent colonic mucus barrier in active and quiescent ulcerative colitis and Crohn's disease," Int. J. Clin. Pract. **62**(5), 762–769 (2008).
50. M. J. Goodman, P. W. Kent, and S. C. Truelove, "Glucosamine synthetase activity of the colonic mucosa in ulcerative colitis and Crohn's disease," Gut **18**(3), 219–228 (1977).
51. S. Heimerl, C. Moehle, A. Zahn, A. Boettcher, W. Stremmel, T. Langmann, and G. Schmitz, "Alterations in intestinal fatty acid metabolism in inflammatory bowel disease," Biochimica et Biophysica Acta (BBA) - Molecular Basis of Disease **1762**(3), 341–350 (2006).
52. T. Smith, R. S. Rana, P. Missiaen, K. D. Rose, A. Sahni, H. Singh, and L. Singh, "High bat (Chiroptera) diversity in the Early Eocene of India," Naturwissenschaften **94**(12), 1003–1009 (2007).
53. M. Rosengarten, N. Hadad, Y. Solomonov, S. Lamprecht, and R. Levy, "Cytosolic phospholipase A2 α has a crucial role in the pathogenesis of DSS-induced colitis in mice," Eur. J. Immunol. **46**(2), 400–408 (2016).
54. T. Minami, H. Tojo, Y. Shinomura, Y. Matsuzawa, and M. Okamoto, "Increased group II phospholipase A2 in colonic mucosa of patients with Crohn's disease and ulcerative colitis," Gut **35**(11), 1593–1598 (1994).
55. W. Stremmel, A. Braun, A. Hanemann, R. Ehehalt, F. Autschbach, and M. Karner, "Delayed release phosphatidylcholine in chronic-active ulcerative colitis: a randomized, double-blinded, dose finding study," J. Clin. Gastroenterol. **44**(5), e101–e107 (2010).
56. W. Stremmel, R. Ehehalt, F. Autschbach, and M. Karner, "Phosphatidylcholine for steroid-refractory chronic ulcerative colitis: a randomized trial," Ann. Intern. Med. **147**(9), 603–610 (2007).

Biomedical Optics EXPRESS

57. M. Karner, V. Schmieg, A. Hanemann, A. Zahn, A. Braun, H. Karner, U. Merle, R. Ehehalt, and W. Stremmel, "T1144 Results of a long-term follow-up treatment with delayed release phosphatidylcholine in chronic-active ulcerative colitis," Gastroenterology **134**(4), A493 (2008).

1. Introduction

Ulcerative colitis (UC) is one of the major forms of inflammatory bowel disease (IBD). It is characteristic of chronic inflammation with continuous disease involvement of the colonic mucosa. In the United States, UC affects approximately 900,000 Americans, with the annual incidence ranging between 2.3 and 15.6 per 100,000 people [1]. Without maintenance treatment, 70% of UC patients can expect to experience a relapse within a year [2, 3]. Due to the chronic relapsing behavior of UC, it is important to keep the disease in remission with optimal therapeutic strategy. To that end, accurate assessment of disease activity is a prerequisite for patient care and treatment response evaluation.

Generally disease activity is determined by endoscopic and histologic evaluation in combination with clinical parameters. Endoscopic mucosal healing is a critical prognostic feature, and has been recognized as a new target of therapy. Mucosal healing is defined by the absence of erosions and ulcerations in all segments of colonic mucosa [4]. Complete mucosal healing has been associated with lower risk of colectomy, hospitalization, relapse, and colorectal cancer [5, 6]. Many endoscopic indices, such as the UC Disease Activity Index and the Mayo Score, have been used to assess disease activity in UC. However, subjective measures of the lesions could lead to large inter-observer variations. Furthermore, endoscopically-determined remission have frequently been identified with histological inflammation [7], which is a proven predictor for clinical relapse and risk factor for colorectal neoplasia [8, 9]. Therefore, it is important to evaluate disease activity both endoscopically and microscopically. Implementing a noninvasive technique that can determine histological inflammation *in situ* during endoscopy could provide a complete evaluation of disease activity and thus offer more reliable guidance for therapy development and disease management.

Raman spectroscopy is an optical technique, that detects the molecular composition in the samples. It can provide diagnostic information based on disease-induced structural and compositional changes in the tissue. Our group has previously applied Raman spectroscopy to characterize epithelial changes in colon mucosa in UC and Crohn's colitis *in vitro*, the two main subcategories of IBD. The relative content of protein and lipid in the tissue has been identified as a promising measure for inflammation assessment [10, 11]. Recently we developed an endoscope-coupled Raman spectroscopy that can provide *in situ* tissue biochemistry analysis during standard colonoscopy procedure [12–15]. The endoscopic Raman technique offers molecular information to differentiate UC and Crohn's colitis, demonstrating great promise in optical diagnosis. In this study, we further investigated the feasibility of applying endoscopic Raman spectroscopy to provide objective assessment of disease activity in UC.

A cross-sectional clinical study was performed to test patients with UC and healthy controls using endoscopic Raman. The acquired Raman spectra were analyzed and correlated with the disease activity of UC assessed by histological analysis on tissue biopsies from the same locations. We discovered distinct spectral markers that are related to the inflammatory status of the tissue. Multivariate statistical analysis showed significant correlation between the markers and histologic inflammation. To the best of our knowledge, this represents the first *in vivo* Raman application for the quantification of disease activity in UC.

2. Experiment

Patient enrollment and information: The present study was conducted with approval by the Institutional Review Board of the University of Texas Health Science Center at Houston. Patients scheduled for surveillance and screening colonoscopy in Memorial Hermann

Biomedical Optics EXPRESS

Hospital at Texas Medical Center (Houston, TX) and the Lyndon B. Johnson Hospital (Houston, TX) were recruited to receive endoscopic Raman measurement during the standard procedure for colonoscopy.

Two cohorts were investigated: one with UC, and one with control patients. The UC cohort consisted of 18 patients with previous diagnosis of UC (10/8 female/male, mean age = 36.6 in the range of 18 - 66), while the age-matched control cohort consists of 31 patients (18/13 female/male, mean age 49.4 in the range of 28 – 60 years) without previous diseases in GI tract.

After endoscopic Raman tests on UC patients, colon tissue biopsies were obtained from the same locations as spectra acquisition. The relevant biometric variables and medical history were retrieved from the patients' electronic medical record (EMR) with consent. The body mass index (BMI) for each patient was calculated based on the body weight and height in the EMR using the formula below, and obesity status is defined by the range of BMI value [16]: underweight (BMI < 18.5); normal (18.5 – 24.9); overweight (25.0 – 29.9); obese (30.0 – 39.9); morbid obesity (BMI > 40.0). No patients were underweight or morbid obese in this study.

$$BMI = \frac{Weight\ in\ kg}{(Height\ in\ meter)^2}$$

Raman instrument: A portable Raman spectroscopy system (Fig. 1(A)), consisting of a monochromic laser source at $\boldsymbol{\lambda}$ = 785 nm (Innovative Photonic Solutions, NJ), a high-throughput holographic spectrograph (Kaiser Optical Systems, MI), a thermoelectric-cooled (–70°C) charge-coupled device (CCD) detector (Princeton Instruments, NJ), and a custom-designed Raman probe (EmVision LLC, FL) was exploited in this study for clinical testing following previously established standard of operation [13]. The fiber optic Raman probe has a 7-around-1 configuration, comprising of 1 center illumination fiber with a bandpass filter to deliver laser light to the sample surface, and 7 surrounding collection fibers with long pass filters to collect Raman scattering signals (Fig. 1(A)). A miniature converging lens was built in to the tip of the probe, which allows for an effective depth of tissue sample to ~800-1000 μm [12] and maximized signal acquisition from colonic mucus layer and colon mucosa [15]. With an outer diameter of 2.2 mm, the fiber optic probe can be easily coupled to the accessory channel of a standard endoscope for data collection [13]. The instrument was calibrated daily for spectral dispersion using the atomic emission lines of a Neon lamp, and for Raman shift calibration using spectra from standard compounds like acetamidophenol and naphthalene [15].

Endoscopic Raman Measurement: Details about endoscopic Raman measurement have previously been depicted [13]. Briefly, the standard operating procedure for colonoscopy was followed for endoscopic inspection of colon surface. As a part of the prognosis (surveillance) procedure for UC patients, colon biopsies were obtained at five anatomical locations of colon, including cecum, ascending colon, transverse colon, descending colon, and rectum. Before biopsy collection at the targeted sites, Raman probe was inserted through the accessory channel of the endoscope, and placed in gentle contact with the colon surface. Although operational variance such as contact pressure and probe-tissue angles do not result in distinguishable spectral variance [17, 18], the participating gastroenterologists were trained to exert only mild pressure on the tissue surface following established standard of operation [15]. At each location, two Raman spectra were acquired at neighboring sites with 3-second exposure time and a laser power of 80 mW at the surface of the tissue. Given the strong contribution of background and tissue autofluorescence to the resulting spectra, the total exposure time of 3 seconds was achieved by multiple accumulations of shorter integration time (250 ms) to reach a high signal-to-noise ratio for later quantitative calculation. Previous Raman study on a cohort of normal subjects revealed no significant differences between the two consecutive spectra in proximity, suggesting the repeatability of the measurements [15].

Biomedical Optics EXPRESS

Residual fecal matters were flush-cleaned with saline solution before *in vivo* Raman measurements. For control patients, spectra were obtained at the five anatomical locations without collection of biopsies.

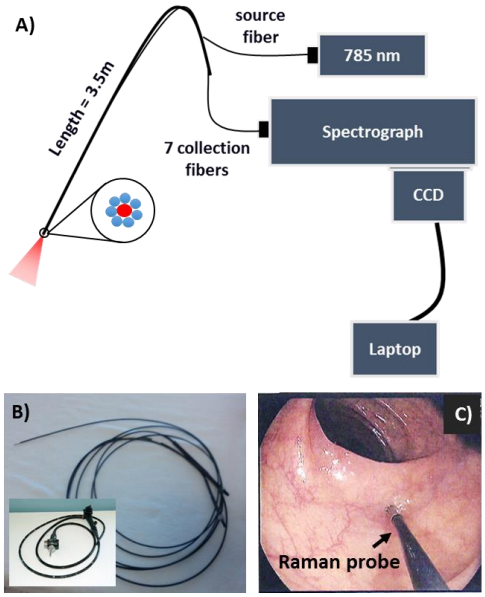

Fig. 1. (A) Scheme of the portable Raman system and the fiber optic Raman probe for endoscopic analysis of tissue composition; The inset shows the configuration of the probe with 1 center fiber for laser delivery (red) and 7 surrounding fibers for data collection (blue). (B) Picture of the Raman probe and the standard endoscope (inset). (C) Raman probe in contact with the surface of the colon after traveling through the accessory channel of the endoscope.

Histology grading: Haemotoxylin and Eosin (H&E) stained histology slides and pathology reports for enrolled patients were requested from the pathology division of the participating hospitals, i.e. MMH and LBJ. The slides were reviewed by an experienced board certified GI pathologist, and scored for disease activity. The scoring system based on modified Riley histological indices was adopted due to its simplicity in grading and reproducibility in outcomes (Table 1) [19].

Table 1. Histological grades of disease activity and the corresponding histological features [19]

Grade	Disease Activity	Histological Features
0	Inactive	No extravascular neutrophils
1	Mild	Neutrophils in the lamina propria
2	Moderate	Cryptitis/crypt abscesses
3	Severe	Erosions/ulcers

Data processing and analysis: Raman spectra were preprocessed to remove tissue autofluorescence using a fifth order polynomial fitting [20], followed by baseline correction using cubic spline interpolation for consistency in peak height calculation and further quantitative analysis [21, 22]. Noise reduction was performed on the baseline corrected spectra with a second-order Savitzky-Golay smoothing filter. The intensity and peak position of major Raman bands were calculated using custom scripts in MATLAB (MathWorks, Natick, MA). To compare intensity differences from different subjects, all the major peak heights were taken ratio to the intensity of Raman band at 1003 cm^{-1} (phenylalanine in proteins), which normalizes the abundance of represented molecules (mainly lipids in this study) to protein level in the sample and thus minimizes inter-sample variability. One-way analysis of variance (ANOVA) was conducted using SPSS Statistics software (IBM SPSS,

Biomedical Optics EXPRESS

Armonk, New York) to determine the statistical significance of differences among the groups of disease activity, followed by Tukey honest significant difference (HSD) post-hoc analysis. Spearman's correlation was conducted to evaluate the association between spectral parameters and histological disease activity. The inflamed tissue group consists of pooled data from grades 1, 2 and 3. An outcome with $p < 0.05$ is considered statistically significant.

3. Results

Histologic assessment: The H&E stained slides for all the tissue biopsies from the UC patients were analyzed for histopathological grading on inflammatory activity. Figure 2 showed the representative H&E images from colon tissue biopsies with histologic scores ranging from 0 to 3. As shown in Table 1, grade 0 referred no disease activity observed in the tissue, i.e. the quiescent, or inactive colitis; whereas grade 1, 2, and 3 meant mild, moderate, and severe inflammation, respectively. The histologic grade 1 is less common in the studied population, and only limited biopsies were graded to that category. Biopsies with nonspecific disease features were excluded from the study.

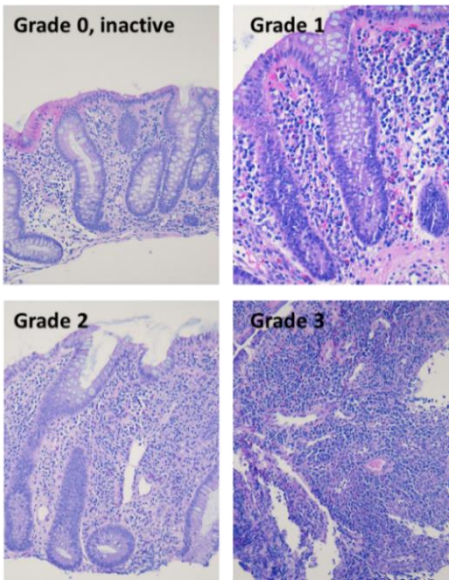

Fig. 2. H&E images of colon tissue biopsies with histology grades of 0 (A), 1 (B), 2 (C), and 3 (D).

Analysis of Raman spectra: Raman spectra under investigation were acquired from the same locations where tissue biopsies were obtained and histologically evaluated. Only Raman spectra that can be co-registered with a definite histologic grade of inflammatory activity were included in the analysis. The spectra were sorted by the histology grades. Figure 3 showed the mean Raman spectra collected *in vivo* from the normal (n = 233) and the colitis colon tissue with histologic grades of 0 (n = 27), 1 (n = 6), 2 (n = 89), and 3 (n = 56) from 31 controls and 18 UC patients respectively. For clear comparison, all the spectra were normalized to the peak height of phenylalanine at 1003 cm^{-1}, arising from proteins in the tissue. As a result, comparison of the intensities from other Raman bands will be relative to tissue protein level, which serves as an internal reference to account for potential inter-sample variability. The peak positions for selected Raman bands are labeled on the spectra, and the tentative molecular assignments are listed in Table 2.

Biomedical Optics EXPRESS

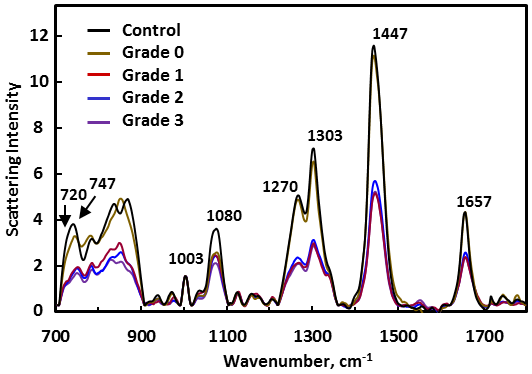

Fig. 3. Mean Raman spectra (normalized to the intensity at 1003 cm^{-1}) from UC patients with different disease activity and from the healthy controls.

Table 2. Tentative assignments for the major Raman bands in colon tissue [23–29]

Raman band, cm^{-1}	Vibration mode	Molecular Assignment
720	Choline ($RN^{+}(CH_3)_3$) stretching	Phosphatidylcholine
750	Ring breathing	Tryptophan, DNA
830, 853	Tyrosine ring breathing	Protein
875	C-C symmetric stretching	Protein and lipids
875, 877	Choline group stretching	Phosphatidylcholine
1003	Phenylalanine ring breathing	Phenylalanine
1068, 1128	Trans C-C stretching	Backbone of lipid, protein, carbohydrate
1080	PO^{2-} group in DNA and lipids	DNA, phospholipids
1086	gauche C-C stretching	Backbone of lipid, protein, carbohydrate
1230-1285	Amide III	Protein
1270	= C-H deformation	Lipids
1303	CH_2 twisting	Lipids
1342	CH deformation	Protein
1447	CH_2 scissoring	Lipid and protein
1600-1700	Amide I α-helix	Protein
1655	Cis -C = C- stretching	Lipid
1735	Ester carbonyl stretching	Lipid

Gross comparison of Raman spectra revealed substantial differences between spectra from inflamed tissue (grade 1-3) and those from the control and inactive UC (grade 0). The most characteristic differences are in the following spectral regions: 700 - 900 cm^{-1}, 1050 - 1100 cm^{-1}, 1200 - 1350 cm^{-1}, 1400 - 1500 cm^{-1}, 1600 - 1700 cm^{-1}. The Raman shift at ~720 cm^{-1} appears as a shoulder in the broader band from 700 – 768 cm^{-1} together with the peak at 747 cm^{-1}. The former (720 cm^{-1}), correlated to the peak at 1303 cm^{-1} (CH_2 twisting in lipids), is

Biomedical Optics EXPRESS

characteristic of the choline group ($R\text{-}CN^{+}(CH_3)_3$) in phospholipids, specifically phosphotidylcholines (PCs). The other choline-specific peak at ~870 cm^{-1} overlaps with the backbone –C-C- stretching from lipids and proteins, and the ring breathing modes from Tyrosine and DNA. Therefore the peak height at 720 cm^{-1} was used to quantify the abundance of PCs in this study.

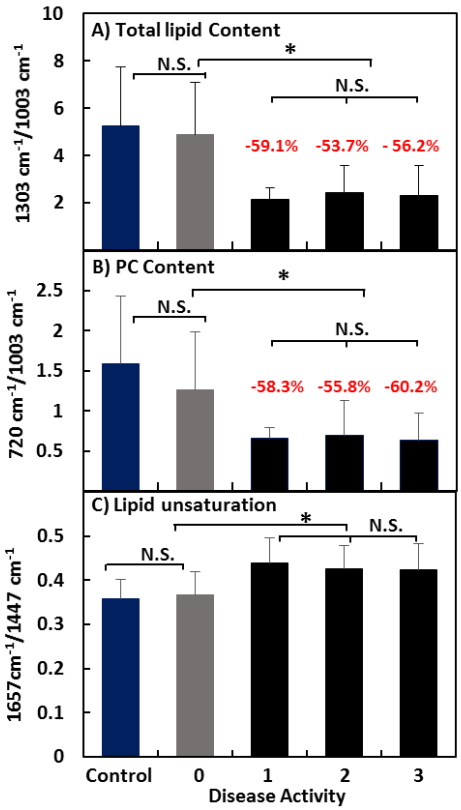

Fig. 4. The content of total lipids (A) and PCs (B) relative to proteins determined by peak height ratios of 1303 cm^{-1} to 1003 cm^{-1} and 720 cm^{-1} to 1003 cm^{-1}. C) The degree of unsaturation in lipids determined by the ratio of n(–C = C-)/n(CH_2), i.e. peak height ratio of 1657 cm^{-1} to 1447 cm^{-1}. * $p<0.01$, N.S.: not significant.

Raman scattering at ~1080 cm^{-1} comprises overlapping contributions from the PO^{2-} group in DNA and phospholipids as well as the backbone stretching from lipids, proteins, and carbohydrates. Given the complex origin of this band, it was excluded from further quantitative analysis. Other spectral features that showed marked differences consist of overlapping assignments from lipids and proteins, but could be differentiated by comparing the band shape and the peak height in relation to other relevant peaks. The broad contour in the range of 1200 – 1350 cm^{-1} generally attributes to the amide III stretching modes from mixed conformations of proteins. With the increasing amount of lipids in the sample, amide III is buried under the strong doublet at 1270 cm^{-1} and 1303 cm^{-1}, which are characteristic of lipids. Both amide I band (1655 cm^{-1}) in proteins and the –C = C- stretching mode (1660 cm^{-1}) in lipids contribute to the Raman feature in the range of 1600-1700 cm^{-1}. A dominant lipid contribution often yields a narrower and more intense peak than the broad and weak amide I band. Similarly Raman feature at 1447 cm^{-1} attributes to the CH_2 scissoring vibration from lipids and the side chains of proteins. In this study, the intensities of the narrow band at 1657 cm^{-1}, the strong vibration at 1447 cm^{-1}, and the characteristic doublet are significantly

Biomedical Optics EXPRESS

related (r^2 = 0.95 – 0.99, $p < 0.001$), indicating these Raman features mainly arose from lipids in the tissue.

Tissue composition analysis: Based on the intensities of these bands, analysis of lipid abundance can be performed. It is evident from spectral comparison that all the Raman peaks from lipids (1270, 1303, 1447, 1657 cm^{-1}) and PCs (720 cm^{-1}) are markedly weaker for tissue with active disease activity, i.e. grade 1, 2 and 3. Ratiometric analysis was performed on the content of PCs (720 cm^{-1}) and total lipids (1303 cm^{-1}) relative to protein (1003 cm^{-1}) (Fig. 4(A)-4(B). The inflammatory groups (grade 1, 2 and 3) showed significantly less amount of lipids (Fig. 4(A)) and PCs (Fig. 4(B)) than the inactive group (grade 0) and the healthy controls. A reduction of 50-60% in lipids and PCs was observed for the inflamed tissue compared to the control, regardless of the severity of the inflammation. No significant difference in lipid or PC content was observed between the control and grade 0, nor among grades 1, 2, and 3.

The degree of lipid unsaturation was determined by calculating the ratio of *n*(-C = C-)/*n*(CH2), i.e. peak height ratio of 1657cm^{-1}/1447 cm^{-1} [27, 30]. Compared to the healthy controls, lipid unsaturation increased around 20% in all of the inflamed tissue regardless of disease severity, but not in the inactive disease group (grade 0).

When data from the inflamed tissue are pooled (grades 1, 2 and 3) and compared with the inactive or control, there is significant correlation between lipid or PC content and the histological assessment of inflammatory status. The Spearman's correlation co-efficient is 0.50 ($p < 0.001$) and 0.61 ($p < 0.001$) for total lipids and PC respectively.

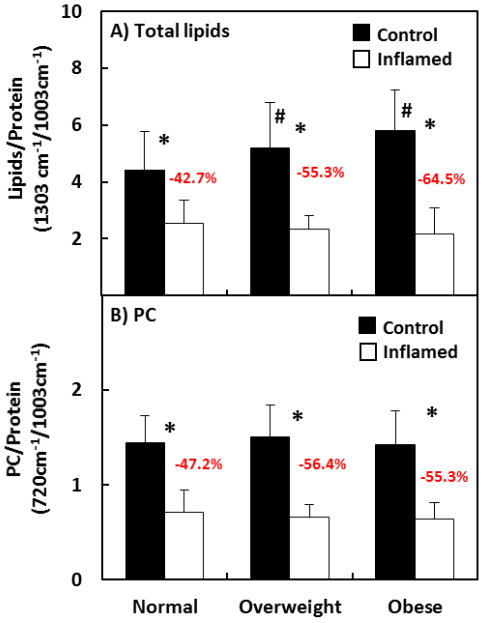

Fig. 5. Comparison of lipids and PC content between control and inflamed colon tissue for different BMI categories. The percentage of decreases in the inflamed groups compared to the BMI-matched controls are marked on the figure. *$p < 0.001$ comparison of control and inflamed tissue; $p < 0.05$ comparison of overweight or obese control and normal-weighted control.

Effect of physiological variability on disease-related changes: We have previously discovered that the BMI status of healthy control is related to the lipid content in colon tissue [15]. The obese and overweight patients showed significantly higher amount of relative lipid content when compared to the normal control (by BMI) [15]. To investigate whether BMI status contributed to disease-associated lipid variance, we stratify all the spectra from active

Biomedical Optics EXPRESS

UC including grades 1, 2 and 3 based on BMI, followed by paired comparison with the controls in the same BMI categories. Although lipid content increased with BMI in the controls, no significant difference was observed among BMI groups in UC patients (Fig. 5). For subjects with normal BMI, the surrogates for PC (720 cm^{-1}) and total lipids respectively reduced 42.7% and 47.2% in UC patients than the healthy control. The overweight and the obese UC subjects demonstrated even higher reduction in PC and total lipids content, 55.3% and 64.5% respectively, than the BMI-matched controls.

The relative content of lipids and protein in normal subjects could significantly vary among different segments of the colon [15, 31]. Lipid contents were compared between normal and inflamed colon tissues as a function of the anatomical locations for data collection (Fig. 6). The contents of total lipids and PC in the rectum of healthy controls are significantly lower than those in other segments of the normal colon, i.e. cecum, ascending colon, transverse colon, and descending colon, which is in agreement with previous publication [15,31]. Compared to the control, both total lipids and PC markedly decreased in inflamed tissue at all the anatomical segments, although the extent of reduction is relatively weaker at the rectum than other locations.

Multivariate classification analysis: We further investigated the feasibility of delineating inflammatory tissue from the inactive and normal tissue using multivariate analysis on the full range of the spectra. Figure 7 shows the receiver operating characteristic curve, or ROC curve, from the support vector machine (SVM) multivariate classifications. The inflamed tissue, containing pooled data of grade 1-3, can be differentiated from the normal or the remission (grade 0) with a sensitivity of 83.5% and 97.1% respectively. ROC-analysis with disease activeness as variable yielded the total area under curve (AUC) of 0.92 between controls and inflammatory tissue (pooled grades 1-3), 0.83 between inactive (grade 0) and active inflammation, and 0.87 between pooled grade 0 and control and active inflammation. These results indicate the potential of determining microscopic inflammation status based on Raman spectral analysis.

4. Discussion

In the current study, we reported *in vivo* composition analysis on colonic tissue in healthy controls and UC using an endoscopic Raman spectroscopy, followed by co-registration with histologic evaluation on biopsies acquired from the same locations. Spectral markers from PCs and lipids have been identified to be related to histologic disease activity in UC. Colon tissue with microscopically active inflammation demonstrated substantially lower amount of lipids and PCs than the control, suggesting that reduction in lipid content is related to the presence of active inflammation in colonic mucosa. On the contrast, the tissue with inactive disease activity (grade 0) showed comparable lipid amount with the control, indicating recovery of lipids in inactive colitis. Such inflammation-associated decrease in lipids is independent of BMI and the anatomical locations, showing the same trend in obese, overweight, and normal-weight subjects. Currently microscopic inflammation status can only be determined by histologic analysis on tissue biopsies. This study offers spectral markers that could be utilized as new endoscopic measures for *in situ* assessment of inflammatory activity in UC.

Biomedical Optics EXPRESS

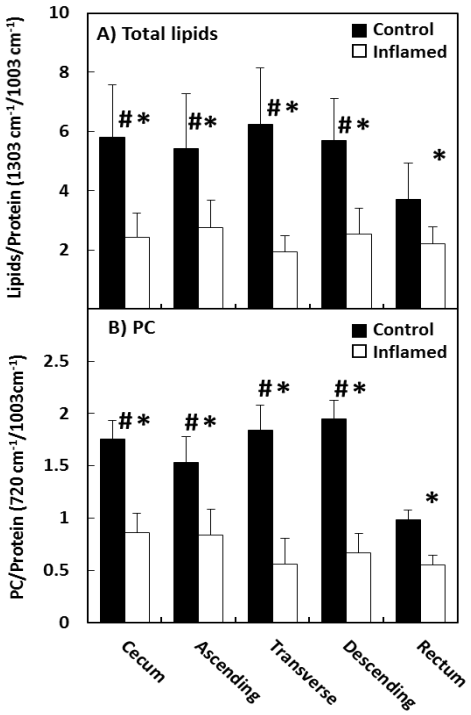

Fig. 6. Comparison of lipids and PC abundance between control and inflamed tissue at different segments of colon, including cecum, ascending colon, transverse colon, descending colon and rectum. * $p < 0.001$, paired comparison between control and inflamed tissue; $p < 0.001$, locations in comparison with rectum.

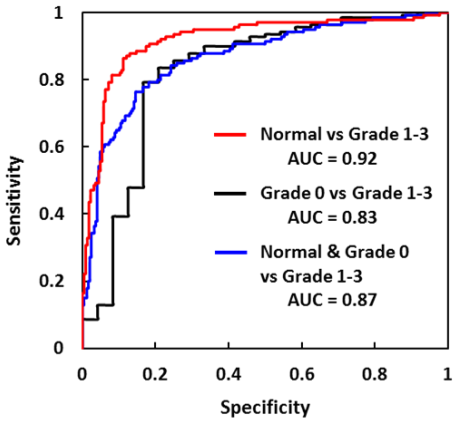

Fig. 7. ROC curve for Raman spectra with histological grading on disease activity as covariate.

Endoscopic Raman spectroscopy can be routinely implemented for biochemical analysis in the gastrointestinal tract *in situ* during standard endoscopy. While most of current quantitative methods for tissue composition such as mass spectrometry are *in vitro* tests requiring tissue biopsies, Raman spectroscopy has significant advantages for its noninvasive nature and no needs for biopsies. The collection of each Raman spectrum *in vivo* can be completed within 0.5s to 3s. As a result, examining the whole colon adds less than 5 minutes to the whole colonoscopy procedure. Due to the clear advantages of this technique, our group and others have applied it for the *in vivo* diagnosis of IBD and colorectal cancer [12–14, 32–34]. Previous works that involved UC focused on the differentiation of UC and Crohn's

Biomedical Optics EXPRESS

colitis, which are two major forms of IBD. When Raman spectra were compared among UC, Crohn's colitis and the controls, the two disease entities displayed similar spectral features in terms of band-shapes, peak positions and relative intensities of major Raman bands to the controls [12–14]. The subtle spectral differences were significant enough for multivariate analysis methods to classify the spectra to the appropriate disease groups correctly, but not applicable for empirical univariate analysis on peak heights. When spectra were further stratified by inflammatory status, a significant improvement was observed in the sensitivity and specificity of classification between the disease groups [14]. Furthermore, although direct spectral comparison between active UC and the normal or the inactive UC was not presented, decrease in the intensities of lipid bands is still evident by visually comparing the spectra side-by-side in the paper [14], supporting the results from the current study. The spectral features in this study are not identical to the previous paper [14] in the region between 1000 cm^{-1} – 1150 cm^{-1} as reflected by a better resolved Raman band at 1003 cm^{-1} in this study, which could result from improved signal-to-noise ratio due to longer total exposure time (3s vs 750ms) per collection and potential contribution from the different baseline correction method employed in the current study.

Our endoscopic Raman system has been designed to detect analytes within an effective depth of ~800-1000 μm into the tissue [12, 15]. The epithelial tissue in colon mucosa is protected by a continuous mucus layer with a thickness of ~830 μm in human [35]. Therefore in the current study Raman scatterings mainly arise from molecules in the compressed mucus layer and colon mucosa. The mucus layer exerts the first line of defense against the penetration of microbe and pathogen in gut lumen. The gel-forming glycoprotein mucins form the main body of the mucus layer, consisting of a dense adherent layer (~116 μm) and a loose outer layer [35, 36]. Whereas surface active lipids, or phospholipids, form a hydrophobic barrier at the luminal surface of colon to protect tissue from the high concentration of water-soluble toxins and bacterial products in the lumen [37, 38]. The mucosal surface of colon is highly hydrophobic [39]. For UC patients, surface hydrophobicity is significantly lower than the control, indicating reduction of lipids at the colon surface in UC [40]. Besides our Raman study, concentration in mucus phospholipids was also quantified by nano-electrospray ionization tandem mass spectrometry (ESI-MS/MS). PCs, representing the major category of phospholipids in the mucus, showed significantly lower concentration (up to 70%) in colonic mucus biopsies from UC patients than those from controls as analyzed by ESI-MS/MS [41, 42]. The present study found 55-60% reduction in PC content at inflamed locations *in vivo*, and similar extent of decrease in phospholipids was observed in an *in vitro* Raman study on colon tissue biopsies from UC [43]. These results demonstrated good agreement between Raman analysis and ESI-MS/MS. In addition, the concentration of mucus PC was reported remaining low for UC patients with endoscopic mucosal healing [41,42], but showed recovery to the control levels for those with histologic healing in our study. Taken together, these studies indicate that loss of mucus lipids might be an intrinsic feature related to inflammation in UC.

In our quantitative analysis, the amount of lipids (and PC) was calculated by normalizing lipid (and PC) content to the level of protein. The dominant protein in colonic mucus layer is mucins, which form a complex network to prevent the invasion of bacteria. The thickness of mucus layer is determined by the dynamic equilibrium between secretion of mucins and its removal into the lumen [44]. For mild and moderate UC, the synthesis of secretory mucins in UC was controversially reported, showing all directions -no change [45, 46], increase [47] or decrease [48] - in the cultures of tissue biopsies when compared to healthy controls. However, the thickness of the adherent mucus gel was found generally lower or unchanged [44, 49], possibly due to excessive removal. In severe UC, both synthesis of mucins and the thickness of mucus barrier substantially declined [48–50]. The decreased mucin levels confirmed that the lower lipid/protein ratio in UC is due to an even larger scale of reduction in lipids. The alterations in mucus thickness, especially in severe UC, could lead to sampling difference by

Biomedical Optics EXPRESS

endoscopic Raman method. However, the phenotypic changes in lipid content (relative to protein) in active UC remain valid as a spectral marker for inflammatory status.

The mechanism for the alterations of phospholipids in UC are still poorly understood. The synthesis of phospholipids starts with phosphatidic acid that is produced from long chain fatty acid via fatty acyl coenzyme A-dependent reactions. Fatty acid synthase was reported down-regulated in UC [51], which could contribute to the reduced phospholipid content. In addition, phospholipase A2 (PLA2) that catalyzes the degradation of PC to lysoPC [52], showed elevated content and activity in animal models of colitis and in actively inflamed colonic mucosa of UC patients compared to the inactively inflamed mucosa and the control [53–56]. The upregulation of PLA2 is consistent with the higher lysoPC-to-PC ratio in UC despite decreased overall PC content (lysoPC + PC) [57].

The elevated unsaturation level in active UC in this study indicates a relative increase in the presence of unsaturated lipids, which could be due to reduction in the amount of lipids with higher saturation degree or actual increase in the amount of more unsaturated lipids. While the mechanism behind such changes remains unclear, it could possibly result from altered fatty acid metabolism in UC. The down-regulation of fatty acid synthase in UC patients could possibly account for the increased unsaturation degree in lipids [51]. Further investigation into the biosynthesis and metabolism of lipids and fatty acids could help elucidate the interplay between lipid alterations and tissue inflammation.

In summary, the current study discovered important Raman spectral markers that are related to histological disease activity of ulcerative colitis. Implementing multivariate analysis on the spectra data set could sensitively differentiate the inflammatory status in UC. Future study with a larger cohort of UC patients is needed to further increase the power and accuracy of multivariate classification. This work suggests the potential of lipid markers along with endoscopic Raman spectroscopy for noninvasive disease assessment of UC *in situ*.

Funding

This work was supported by the Broad Medical Research Program at the Crohn's & Colitis Foundation of America [IBD-1330], and in part by NIH grant DK056338, which supports the Texas Medical Center Digestive Diseases Center.

Conflict of Interest

The authors have no conflict of interest to declare.